PROCEEDINGS OF SPIE

SPIEDigitalLibrary.org/conference-proceedings-of-spie

Planning in-flight calibration for XRISM

Miller, Eric, Sawada, Makoto, Guainazzi, Matteo, Simionescu, Aurora, Markevitch, Maxim, et al.

Eric D. Miller, Makoto Sawada, Matteo Guainazzi, Aurora Simionescu, Maxim Markevitch, Liyi Gu, Megan Eckart, Caroline Kilbourne, Maurice Leutenegger, F. Scott Porter, Masahiro Tsujimoto, Cor de Vries, Takashi Okajima, Takayuki Hayashi, Rozenn Boissay-Malaquin, Keisuke Tamura, Hironori Matsumoto, Koji Mori, Hiroshi Nakajima, Takaaki Tanaka, Yukikatsu Terada, Michael Loewenstein, Tahir Yaqoob, Marc Audard, Ehud Behar, Laura Brenneman, Lia Corrales, Renata Cumbee, Teruaki Enoto, Edmund Hodges-Kluck, Yoshitomo Maeda, Paul Plucinsky, Katja Pottschmidt, Makoto Tashiro, Richard Kelley, Robert Petre, Brian Williams, Hiroya Yamaguchi, "Planning in-flight calibration for XRISM," Proc. SPIE 11444, Space Telescopes and Instrumentation 2020: Ultraviolet to Gamma Ray, 1144426 (13 December 2020); doi: 10.1117/12.2561608

SPIE.

Event: SPIE Astronomical Telescopes + Instrumentation, 2020, Online Only

Planning in-flight calibration for XRISM

Eric D. Miller[a], Makoto Sawada[b], Matteo Guainazzi[c], Aurora Simionescu[d], Maxim Markevitch[e], Liyi Gu[b], Megan Eckart[f], Caroline Kilbourne[e], Maurice Leutenegger[e], F. Scott Porter[e], Masahiro Tsujimoto[g], Cor de Vries[d], Takashi Okajima[e], Takayuki Hayashi[e,h], Rozenn Boissay-Malaquin[e,h], Keisuke Tamura[e,h], Hironori Matsumoto[i], Koji Mori[j], Hiroshi Nakajima[k], Takaaki Tanaka[l], Yukikatsu Terada[n,g], Michael Loewenstein[e,m], Tahir Yaqoob[e,h], Marc Audard[o], Ehud Behar[g,p], Laura Brenneman[q], Lia Corrales[r], Renata Cumbee[e,m], Teruaki Enoto[b], Edmund Hodges-Kluck[e], Yoshitomo Maeda[g], Paul Plucinsky[p], Katja Pottschmidt[e], Makoto Tashiro[l,g], Richard Kelley[e], Robert Petre[e], Brian Williams[e], and Hiroya Yamaguchi[g]

[a]MIT Kavli Institute for Astrophysics and Space Research, Cambridge, MA 02139, USA
[b]RIKEN Nishina Center, 2-1 Hirosawa, Wako, Saitama 351-0198, Japan
[c]European Space Agency, European Space Research and Technology Centre, 2200 AG Noordwijk, The Netherlands
[d]SRON Netherlands Institute for Space Research, Utrecht, The Netherlands
[e]NASA/Goddard Space Flight Center, Greenbelt, MD 20771, USA
[f]Lawrence Livermore National Laboratory, Livermore, CA 94550, USA
[g]Japan Aerospace Exploration Agency, Institute of Space and Astronautical Science, Sagamihara, Kanagawa, Japan
[h]University of Maryland Baltimore County, Center for Space Science and Technology, Baltimore, MD 21250, USA
[i]Department of Earth and Space Science, Osaka University, Osaka 560-0043, Japan
[j]Department of Applied Physics and Electronic Engineering, University of Miyazaki, Miyazaki 889-2192, Japan
[k]College of Science and Engineering, Kanto Gakuin University, Kanagawa 236-8501, Japan
[l]Department of Physics, Kyoto University, Kyoto 606-8502, Japan
[m]University of Maryland, Department of Astronomy, College Park, MD 20742, USA
[n]Saitama University, Graduate School of Science and Engineering, Sakura, Saitama, Japan
[o]Department of Astronomy, University of Geneva, Versoix CH-1290, Switzerland
[p]Department of Physics, Technion, Technion City, Haifa 3200003, Israel
[q]Center for Astrophysics | Harvard & Smithsonian, Cambridge, MA 02138, USA
[r]Department of Astronomy, University of Michigan, Ann Arbor, MI 48109, USA

ABSTRACT

The XRISM X-ray observatory will fly two advanced instruments, the Resolve high-resolution spectrometer and the Xtend wide-field imager. These instruments, particularly Resolve, pose calibration challenges due to the unprecedented combination of spectral resolution, spectral coverage, and effective area, combined with a need to characterize the imaging fidelity of the full instrument system to realize the mission's ambitious science goals. We present the status of the XRISM in-flight calibration plan, building on lessons from Hitomi and other X-ray missions. We present a discussion of targets and observing strategies to address the needed calibration measurements, with a focus on developing methodologies to plan a thorough and flexible calibration campaign and provide insight on calibration systematic error. We also discuss observations that exploit Resolve's spectral

Further author information:
E. D. Miller: E-mail: milleric@mit.edu

Space Telescopes and Instrumentation 2020: Ultraviolet to Gamma Ray, edited by Jan-Willem A. den Herder
Shouleh Nikzad, Kazuhiro Nakazawa, Proc. of SPIE Vol. 11444, 1144426 · © 2020 SPIE
CCC code: 0277-786X/20/$21 · doi: 10.1117/12.2561608

resolution to calibrate atomic codes, and cross-calibration between the XRISM instruments and with other observatories.

Keywords: XRISM, Calibration, X-ray Astronomy, IACHEC

1. INTRODUCTION

The X-ray Imaging and Spectroscopy Mission (XRISM)[1,2] is the next major Japanese-led X-ray observatory. XRISM will fly Resolve, a high-spectral-resolution imaging microcalorimeter very similar to Hitomi's SXS; and Xtend, a large-field CCD imager based on Hitomi's SXI. Resolve in particular will expand a new era of spatially resolved X-ray spectroscopy begun by Hitomi[3–17] and expected to be continued by future missions such as Athena[18] and Lynx.[19]

Great efforts are currently underway by the XRISM instrument teams to characterize and calibrate Resolve and Xtend on the ground.[20–22] Despite this care, the stress of launch and harsh environment of space can alter the characteristics of the instruments, requiring both initial calibration once on orbit and regular monitoring and recalibration of various components over the life of the mission. As is the case with all space-based X-ray missions, a robust in-flight calibration plan is required before launch to address these needs. The XRISM instruments, particularly Resolve, pose unique calibration challenges due to the unprecedented combination of spectral resolution, spectral coverage, and effective area, combined with a need to characterize the imaging fidelity of the full instrument system to realize the mission's ambitious science goals.

We here present the status of the XRISM in-flight calibration plan, which is currently in development and takes into account the performance requirements set by the primary mission science goals, the supported instrument operating modes, the status of the ground calibration, the availability of suitable celestial calibration targets, and the required calibration output. The output of the in-flight calibration plan includes two major components: (1) a quantitative justification of the exposure times and strategies to reach the necessary calibration precision; and (2) the method by which the observations will be used to update the calibration files (CALDB) and software algorithms.[23,24] As expected, this plan borrows heavily from the Hitomi plan due to the similarity of the payload, but it differs in some ways due to changes in the instrumentation and ground calibration.

The paper is organized as follows. The calibration requirements are presented in Section 2, along with considerations of scheduling priority and boundary conditions placed on the plan by external forces. Section 3 presents an overview of the plan formulation methodology, including the team structure and lessons learned from Hitomi and other missions. Section 4 provides detailed information about targets and observing strategies. We emphasize that this plan is still in formulation, and due to space constraints it cannot be thoroughly detailed here. The final version implemented after launch may differ in important ways from what is set out below.

2. CALIBRATION REQUIREMENTS

The calibration requirements for XRISM were derived directly from the mission science goals[1,2] by the Instrument Teams.[25] These requirements, shown in Table 1, apply to the in-orbit, fully integrated Resolve and Xtend instruments, in both cases including the X-ray Mirror Assembly (XMA) as an integral part of the instrument, and they must be verified with a full measurement once in space. There are several additional requirements that can only be addressed through sub-system ground calibration and simply spot-checked on orbit, and those are not discussed here. These considerations are all part of the in-flight calibration plan. In addition, constraints imposed by physical limitations ("boundary conditions") of the mission and the necessity to perform certain measurements in a certain sequence all shape the plan. These considerations are addressed below.

2.1 Boundary Conditions

A number of constraints affect the planning and the execution of the in-flight calibration plan. These constraints range from programmatic (data rights issues) to operational (sun angle constraints) to physical limitations of the detectors, among others, and a selection are described below. Clearly, the achievable goals for an in-flight calibration plan depend critically on the allocated time to implement such a plan.

Table 1. XRISM calibration requirements to be verified in flight.[a]

Requirement	Resolve	Xtend
Energy scale	2 eV for each pixel [1 eV (0.05–12 keV), 3 eV (12–25 keV)]	5% (1 keV) 0.3% (6 keV)
Energy resolution (FWHM)	1 [0.5] eV for each pixel[b] [2 eV (12–25 keV)]	10% (1 keV)[c] 5% (6 keV)[c]
Abs. eff. area on-axis[d]	10% [5%]	10% [5%]
Abs. eff. area off-axis[d]	10% [5%] within 5′	15% [10%] within 10′
Rel. eff. area on-axis[d]	5% [3%] [5% (12–25 keV)]	5% [2%]
Rel. eff. area < 2′ off-axis[d]	5% [3%] [5% (12–25 keV)]	10% [5%]
Rel. eff. area 2′–5′ off-axis[d]	10% [10% (12–25 keV)]	10% [5%]
Rel. eff. area > 5′ off-axis[d]	N/A	10% [5%]
Rel. eff. area fine structure[d]	5% in 1 eV bins around C, N, O K edges[e]	15% at Si K edge
PSF on-axis[f]	5% [3% (0.3–25 keV)]	10%
PSF off-axis[g]	5% [5% (12–25 keV)]	[10%]
Absolute timing[h]	1.0 ms	10 ms
Relative timing[h]	0.5 ms	TBD
Aimpoint	Difference in the aimpoint and optical axis known to 30″	

[a] Unless otherwise noted, requirements are 1 σ uncertainties over 0.3–12 keV. Values given in [] are goals.

[b] Knowledge of the Gaussian peak width for hi- and mid-res primary events. Off-peak redistribution components have additional requirements for ground calibration and will be spot-checked if feasible in flight.

[c] Knowledge of the full redistribution width on the on-axis CCD. Off-axis CCDs have no current response calibration requirements.

[d] All effective area requirements apply to all allowed Resolve filter and gate valve combinations. The effective area knowledge in the gate valve closed configuration can be relaxed by 5% precision compared to the requirements in the nominal configuration, and is only applicable to energies above 1.8 keV. The fine structure effective area in these configurations must be calibrated for appropriate K edges (edges of the primary materials and known contaminants) and other known features (e.g., Bragg diffraction features).

[e] Additional requirements apply to ground calibration of filter transmission edges at higher energies. Those shown are relevant to on-orbit monitoring of molecular contamination.

[f] For Resolve, the point spread function (PSF) requirement is defined as the uncertainty in the fraction of photons on each pixel for a source at the aimpoint.

[g] For Resolve, this is defined as the uncertainty in the fraction of photons on each pixel for a source within 2′ of the aimpoint; or in 3×3 corner pixel groups for a source 2′–4′ off-axis.

[h] Timing requirements are defined for the end-to-end satellite timing system; i.e., values include allocations for both the instrument time tagging uncertainty and the spacecraft time coordinate uncertainty. The uncertainty interval that defines the Xtend absolute timing requirement is TBD.

2.1.1 Allocated observing time

The XRISM Operations Concept[23] lays out the operational phases of the mission. For execution of the in-flight calibration plan, the relevant ones after launch are the Initial Phase, which consists of the Critical Operations period and Commissioning period, and the Nominal Operations Phase which consists of Initial Calibration and Performance Verification (PV) period and Nominal Observation period. We assume for the purposes of constructing a realistic plan that the Initial Phase will last 3 months with no formal time allocated for calibration, since the purpose of every operation in this phase is commissioning, function, and performance verification of the spacecraft bus and instruments. To best optimize the use of time in the Initial Phase, the in-flight calibration plan should produce a list of calibration targets that the instrument and operation teams can use for verification purposes. These observations are not guaranteed to be useful for calibration purposes, however. We further assume that the Nominal Operations Phase will comprise a one-month calibration period wholly allocated to in-flight calibration; a six-month PV period during which 5% of the observing time is allocated to initial calibration activities; and an open-ended nominal Guest Observer (GO) phase during which 5% of the observing time is

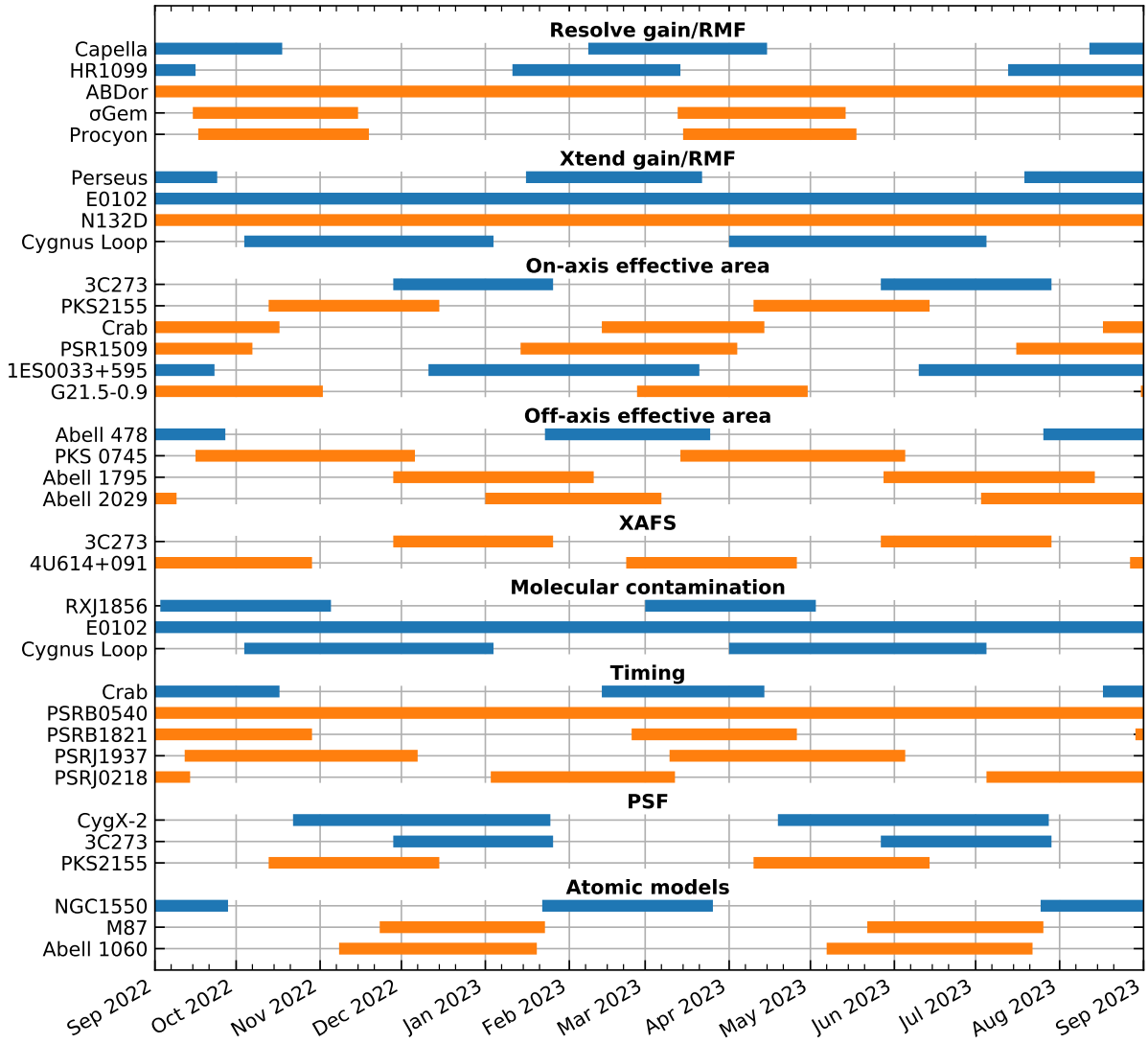

Figure 1. Visibility for XRISM calibration targets during a one-year period around the expected launch and PV phase. Bars indicate when a target is within the $90^\circ \pm 30^\circ$ Sun angle limit. Targets are grouped by calibration category, with blue bars showing primary targets, orange bars secondary targets.

allocated to routine calibration activities. For the seven months of calibration plus PV period, assuming 43% observing efficiency based on Suzaku experience, the total observing time available for in-flight calibration is thus assumed to be about 1.4 Msec. For the GO phase, we assume routine calibration will be allocated about 0.7 Msec per year. The in-flight calibration plan must fit within these total exposure time constraints.

2.1.2 Operational constraints

Constraints are also imposed on the plan by operational limitations of the satellite. The order in which calibration observations are performed as well as which targets are used depend critically on the spacecraft orbital constraints, which determine source visibility. The spacecraft's field of regard is $\pm 30^\circ$ around a 90° Sun angle. This means that sources are observable for two months or longer twice a year. The shortest visibility window is for sources along the Ecliptic, the foremost of which is the Crab. Some candidate calibration sources are at high enough Ecliptic latitude to be continually visible (1E 0102.2−7219, N132D, Vela, AB Dor). The current specification for

the spacecraft roll angle is limited to ±30° degrees. This limitation might matter for optimization of placement on the focal plane for some extended sources or multi-pointing rastering scans. Because of these operational constraints, and the uncertainty of launch date at this point in the project, it is vital to identify secondary calibration sources that can be used if the primary source is not visible when needed. These source visibility windows are shown in Figure 1 and are used to aid the team in this determination.

2.1.3 Instrument capabilities

Finally, instrument limitations must be considered when selecting suitable targets. For example, the maximum count rate of Xtend in Full Window mode[26] is severely limited by pile-up, and this count rate limitation complicates plans for on-orbit verification of the shape of the Xtend point spread fuction (PSF) and cross calibration of the Xtend and Resolve effective area. Similarly, at high count rates pulses begin to overlap and degrade spectral resolution on Resolve, limiting the flux of sources that can be used for calibration measurements, which have much stricter requirements on fidelity than science observations. For very bright sources, the pulse shape processor (PSP)[27] event handling rate and the telemetry buffer size introduce dead time into Resolve.

2.2 Priorities of Time-Sensitive Calibration

Certain calibration measurements will need to be performed as soon as possible after on-orbit activation, because (1) the knowledge or the calibration of the corresponding observable is a precondition for the knowledge or calibration of other parameters characterizing instrument performance, or (2) the measurement enables XRISM to achieve breakthrough scientific results. The following calibration items are identified as the highest priorities, and the corresponding calibration observations are expected to be scheduled as soon as possible during the calibration phase:

1. Determination of the boresight and optical axis position of both instruments.
2. Verification of the accuracy of time assignment.
3. Verification of the accuracy of the Resolve energy scale and resolution.
4. Monitoring campaign of the Resolve (gate valve open) and Xtend effective area in the soft X-ray band to detect possible buildup of ice or other contaminants along the optical path.
5. First characterization (at the 10% level) of the overall effective area calibration and inter-instrument calibration.

Again, due to the time pressure of these calibration observations and the uncertainty of exact launch date at this time, it is vital to identify enough potential targets to satisfy these priorities at any time of year.

3. CALIBRATION METHODOLOGY & LESSONS LEARNED

3.1 Organization

The XRISM In-Flight Calibration Planning (IFCP) team comprises about 30 members of the larger XRISM team, with members drawn from the two Instrument Teams,* the Science Operations Team (SOT),[23,24] and the Science Team. In this way, calibration planning is supported by personnel with the necessary technical and astrophysical background to understand the limits imposed by both the instrumentation and the celestial sources. In many cases there is natural overlap between technical and scientific expertise, but including Science Team members in the planning endeavor enhances the knowledge of source characteristics that could affect calibration measurements, ensures that all interested parties have a stake in proper calibration to reach the desired science goals, and (perhaps most importantly) greatly expands the workforce available to run complex simulations of different calibration strategies and review possible targets.

While the plan for calibration data analysis activities after launch is still in development, we expect that a team of "calibration experts" will be formed under the auspices of the SOT, with many drawn from the same pool of IFCP team and Science Team members, as was the plan for Hitomi. The Instrument Teams will lead the calibration effort, aided by these "calibration experts" who will analyze the data with the aim of producing

*The Resolve team includes by definition members responsible for design, fabrication, testing, and calibration of the XMA for each instrument.

updated calibration files and corresponding documentation. That these members have experience with analyzing X-ray data and extensive knowledge about the limitations imposed by these astrophysical sources is as key for this effort as for the planning, and involving the same people in both the observation planning and data analysis is clearly desirable to ensure efficient and timely construction of calibration products from a large quantity of early data.

3.2 Flexibility

Perhaps the most important lesson learned from calibrating generations of X-ray instruments in space is the need for flexibility. This lesson was realized for the Hitomi in-flight calibration plan, and built on for XRISM. Having a set of primary and secondary calibration targets identified well in advance of launch can ameliorate the effects of unexpected schedule changes, including launch delays. Similarly, it is important to perform simulations of observations and settle on strategies well before launch so that this flexible plan is ready and in place when it is needed. And while it is impossible to anticipate all problems that a mission might encounter on-orbit, we can learn from previous experience and be prepared. For example, given the problems that previous missions such as Suzaku and Chandra have experienced with build-up of molecular contamination, it is vital for XRISM to have not only a plan to regularly monitor for such contamination, but a flexible plan to put in place to characterize and calibrate its effect if it occurs. Such a plan is currently under development (see Section 4.6.2).

3.3 Coordination

Using celestial sources as calibration targets is hampered by the fact that their characteristics are not fully known, but rather inferred from previous observations using other instruments. That these sources are often variable, and that the various instruments studying them can have quite different capabilities and their own calibration issues complicates things further. The goal of the International Astronomical Consortium for High-Energy Calibration (IACHEC)[28†] is to ameliorate these effects by compiling and providing information on standard candles and best calibration practices, and helping to coordinate among missions for variable-flux targets that require simultaneous observations. Many members of the XRISM IFCP team are members of IACHEC, and the XRISM plan naturally leverages the expertise of IACHEC. Indeed, the Hitomi in-flight calibration plan was presented to and vetted by several annual meetings of IACHEC, and such is the expectation for the XRISM plan summarized below.

4. CALIBRATION TARGETS AND STRATEGIES

Here we summarize the current, preliminary XRISM in-flight calibration plan. This section is organized by calibration categories, each of which is under detailed study by a sub-group of the larger IFCP team, although there is clearly overlap between several categories in terms of targets and strategies. Section 4.6 deals with a set of calibration targets and strategies that do not specifically calibrate an instrumental characteristic, but rather improve our understanding of underlying science in order to maximize the impact of many XRISM observations. Of course, many of these targets have interesting science to study beyond the calibration they provide.

4.1 Resolve Energy Scale and Spectral Response

Resolve carries a set of on-board radioactive sources and X-ray generators enabling in-flight calibration of the gain scale and the energy-dependent redistribution function (the line spread function or LSF).

Calibration pixel: There is a calibration pixel near the main calorimeter array but outside the telescope field of view (FOV).[29] The calibration pixel will not receive photons from the sky or other on-board calibration sources, but only from a small, highly collimated ^{55}Fe source mounted above it. The calibration pixel is always on, and its high continuous flux of Mn Kα photons makes it ideal for probing temporal variations in the LSF from changing sources of interference on the spacecraft, and the manifestation on the full array can be inferred from this. It can also be used for monitoring the drift of the energy scale and changes in the LSF core. The calibration pixel has been used extensively for ground testing and calibration.

[†] https://iachec.org

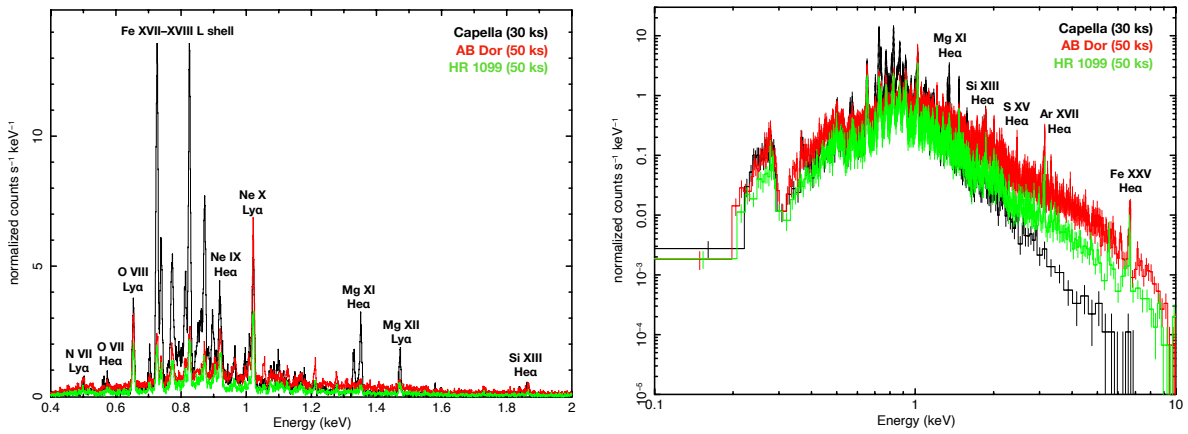

Figure 2. Resolve simulations of bright coronal stars expected to serve as targets for calibrating the energy scale and LSF. The left panel has a linear scale to show the strong low-energy lines, and the right panel shows the same thing on a log scale and to higher energies. Major emission features are identified. Capella dominates at energies less than 2 keV, but as the right plot shows, either AB Dor or HR 1099 are required to provide bright lines above 2 keV.

Filter Wheel ^{55}Fe sources: One of the six filter wheel[30] positions contains a set of ^{55}Fe sources mounted to metal crossbars. These ^{55}Fe sources illuminate the calorimeter array with Mn K photons, providing per-pixel information unavailable using just the calibration pixel ^{55}Fe source. On-orbit, when the gate valve is open, the typical count rate will be 1 count s^{-1} pixel^{-1}.

Direct Modulated X-ray Sources: The direct modulated X-ray sources (MXSs)[30] are mounted near the filter wheel at 180° from each other. The direct MXSs provide pulsed Cr K and Cu K emission lines; they will typically be operated at a 1–3% duty cycle with a period of ∼1 ms and an average count rate of 1–3 counts s^{-1} pixel^{-1}, although this is one choice out of a large range of possible setting. Unlike the calibration pixel, the MXSs illuminate the full pixel array, allowing for pixel-to-pixel monitoring of the energy scale drift and LSF width.

Indirect Modulated X-ray Source: There are two additional MXSs on-board, mounted 180° from one another and 90° from the direct MXSs. These 'indirect' MXSs consist of an MXS pointed not at the array but instead at a nearby Al/Mg target. The resulting fluorescent photons are directed at the calorimeter array, providing Al K and Mg K lines. Because the fluorescence process is not efficient, the flux on the calorimeter array will be much lower in this configuration compared to the direct MXSs for a given set of operating parameters; this will be partially compensated by increasing the MXS intensity. The indirect MXSs cannot be used in the gate valve closed configuration because the Be gate valve window absorbs the low-energy photons.[22]

These X-ray line sources are the basic tools for the in-flight verification of the width of the dominant Gaussian core of the LSF. The intrinsic spectral complexity of astrophysical sources prevents accurate and efficient measurements of the extended instrumental redistribution function. No specific pointing in the in-flight calibration plan is therefore foreseen to verify the intensity of the Hg and Te escape peaks, the flux and shape of the electron loss continuum, the e-folding energy and fractional flux of the LSF exponential tail, and the strength of the Si K fluorescence, as these are all known from ground calibration and are not expected to change. In some cases, serendipitous observations of continuum or heavily obscured sources in the framework of the in-flight calibration or the PV phase can be also used for this purpose.

Additional verification of the energy resolution and of the gain scale will make use of magnetically active low-mass stars. They are strong X-ray emitters with rich emission-line spectra due to collisional ionization equilibrium plasma (see Figure 2). Typical coronal temperatures range from a few MK to several tens of MK. Coronal stars have long been used as spectral resolution and energy scale calibrators for X-ray missions,[31] in particular those carrying grating instruments. Coronal stars have generally narrow emission lines (in contrast, e.g., to massive stars) and display no energy shift (to first approximation). The brightest coronal stars in

Table 2. Achievable gain calibration uncertainty for Xtend.

	Gain uncertainty	$t_{\rm exp}$ **(ks)**	**Description**
Case I	7 eV @ $r < 8'$ 18 eV @ $8' < r < 15'$ 60 eV @ $r > 15'$	80	Observed only on-axis to reach the same gain uncertainy as Suzaku/XIS.
Case II	7 eV on-axis chip 8 eV neighbor chips 9 eV opposite chips	320	Observed on each chip for the same exposure time and goal as Case I. Off-axis chips have higher uncertainty due to vignetting.
Case III	7 eV everywhere	640	Observed on each chip for exposure time that scales with vignetting, to reach the Suzaku/XIS gain uncertainty at all FOV locations.

quiescence are generally RS CVn binaries, with both components being X-ray active. Capella is the brightest in the soft X-ray band (≤ 2 keV). We estimate that 30 ks at the nominal boresight position will yield a statistical precision on the centroid (width) of better than 0.7 (1) eV on the central pixel for several lines or line complexes in the 0.5–2.0 keV band, ranging from N VII Lyα to Mg XII Lyα and the Si XIII Kα complex. To cover the energy range harder than 2 keV, 50 ks of a hotter system such as HR 1099 (primary) or AB Dor (secondary) are needed to achieve a precision of the reconstructed gain scale over the full Resolve energy band better than 1%.

In order to verify the accuracy of the energy scale and resolution over the whole Resolve array, a raster experiment of Capella has been designed. It is constituted by a set of nine observations (for a total exposure time of 40 ks) with slight offsets around the nominal boresight position and covering the whole instrumental field-of-view with a spatial distribution of counts as homogeneous as possible, while ensuring that the strongest Fe L emission lines at $\simeq 0.72$ keV and $\simeq 0.82$ keV are detected with at least 1,000 counts each. As the experiment must be repeated for two instrumental modes and three operational temperatures, the total time investment is estimated to be 240 ks.

4.2 Xtend Energy Scale and Spectral Response

Calibration of the energy scale (gain) and spectral resolution of a CCD detector is technically equivalent to correcting the charge trail and charge transfer inefficiency (CTI) resulting from transfer of charge during readout. Since these depend on the number of transfers, line-emitting, diffuse, bright sources that cover the FOV are required. In the Suzaku XIS case, the Perseus cluster and Cygnus Loop were routinely observed to calibrate the gain and spectral response at high and low energies, respectively, across the FOV. ^{55}Fe calibration sources irradiating the corners of CCD chips were used to monitor the time-dependency of the gain and energy resolution. This observing strategy worked well for Suzaku, and so we base the in-fight calibration plan for Xtend on experience calibrating the Suzaku XIS.

One big advantage for Xtend over the XIS is the capability for simultaneous observations with Resolve, since Resolve spectra of any line-emitting sources would be good references for Xtend. It is thus expected that energy calibration will be more accurate and easier on-axis. On the other hand, the wider FOV of Xtend requires much longer exposure times if the same calibration uncertainty is to be achieved over the whole detector. We show in Table 2 the achievable calibration uncertainty and required calibration time for three cases using the Perseus cluster as a calibration target. The baseline plan is to achieve Case I, which will satisfy the Table 1 gain requirement of 0.3% (18 eV) at 6 keV over half of the FOV, and substantially exceed this on-axis. Thanks to the strength of its He- and H-like Fe K lines near 6 keV, a single 40-ks observation of Perseus at the nominal aimpoint will do this. A 30-ks observation of the Cygnus Loop, a $\sim 3^\circ$ structure that covers all four chips, will allow monitoring of the gain over the whole FOV at energies lower than about 2 keV. Both these observations will be repeated performed in Full Window and 1/8 Window modes. Plans to pursue Case II or III will be explored once Case I is demonstrated in flight.

Alternative sources to the Perseus cluster are X-ray bright clusters such as Abell 478, Abell 1795 and Abell 3571, although they are fainter than the Perseus cluster in the Fe K lines. The Circinus Galaxy is a heavily obscured AGN whose spectrum below 10 keV is dominated by reprocessing of the nuclear radiation by optically

thick matter on scales of the order of a few parsecs,[32,33] and whose emission is expected to be constant over the lifetime of the mission. Since it is point-like, it could be useful for verification of the accuracy of the energy scale reconstruction on-axis. The statistical constraints on the centroid energy of the Fe K line in Cas A are even tighter. However, the complex, diffuse morphology of this target and possible pile-up in the brightest features make it a back-up calibration source. The Vela supernova remnant is a possible alternative to the Cygnus Loop.

4.3 Effective Area

We must calibrate the effective area of Resolve and Xtend in order to allow accurate determinations of the flux and spectral shape of observed astrophysical sources. We also need a proper basis of comparison from which to evaluate a XRISM spectrum against one obtained simultaneously with another X-ray telescope. Therefore, three principle questions must be addressed by our in-flight calibration observations:

1. Do the two detectors onboard XRISM report different spectral values than those expected from pre-launch calculations and ground calibration data, given also the current spectral state of the observed source?
2. If so, how can we characterize and correct for these differences within the framework of the pipeline processing to achieve well-calibrated data products?
3. Are these changes meaningful and consistent in the context of the existing XRISM ground measurements and ray-tracing software?

In preparation for answering these questions after launch, our pre-launch efforts focus on extensive analysis of simulations created with a variety of exposure times and calibration sources. The goal is to determine the accuracy and precision with which we can recover the critical input variables (e.g., flux and spectral slope in a given energy band) in our simulations. This knowledge will inform us about the statistical quality we can expect from the real data for a given exposure time, enabling us to determine the necessary time allocation for meeting the calibration requirements. Any deviations in the fitted spectral parameter values that are outside of our measured statistical uncertainties for that exposure time can then be attributed to either systematic effects (e.g., intrinsic source variation, calibration errors) or, more critically, to degradation in the performance of the detectors (e.g., due to contaminant build-up). Simultaneous observations of these sources with other X-ray telescopes will also be necessary in some cases to determine the possible cause(s) of additional uncertainty.

The main difference with respect to the Hitomi in-flight calibration plan is that XRISM lacks the higher-energy HXI and SGD instruments. As such, the order of priority between various calibration sources must be re-assessed, in particular giving a lower priority to sources with very hard spectra (such as Cen A). Our preliminary target list for the on-axis effective area calibration of Resolve includes the point-like AGN 3C273[34] and PKS 2155−304 (hereafter PKS 2155),[35] with the pulsar PSR 1509−58[36] as a back-up source. These targets have been extensively studied with almost every X-ray telescope over the past four decades (and, in some cases, have been vetted by the IACHEC), and they span a range of visibility windows over the foreseen post-launch time frame (Figure 1). Unfortunately, while their brightness is well-suited for obtaining a detailed spectrum with Resolve, 3C273, PKS 2155, and PSR 1509−58 will all suffer from pile-up in Xtend when observed in Full Window mode. We are currently considering the use of special observing modes (e.g., 1/8-window mode) for these bright targets with Xtend; however, this can introduce additional systematic uncertainties related to the different ratios of dead time and out-of-time events between these modes. Likewise, excising the central core of the PSF as a way of mitigating pile-up introduces uncertainties related to the PSF shape. It is important therefore to include sources that will not be piled up as primary calibrators for Xtend. For this, we are considering 1ES 0033+595,[37] which has a lower flux across the band-pass, and the plerionic SNR G21.5−0.9,[38] whose 4′ spatial extent also helps to mitigate pile-up effects.

Using spectral models taken from the literature, the `SIMX` software package[‡], and the most recent version of the XRISM response files, we have created a suite of simulations of the main targets listed above, assuming an array of 6 different exposure times of 10, 20, 30, 50, 75, and 100 ks, and various Resolve filter configurations: gate-valve closed (assumed to be a short period during the initial phase after launch), open filter, neutral density (ND), and beryllium (Be) filter. Xtend, lacking a filter wheel, has only one optical path configuration. Simulations include

[‡] https://hea-www.harvard.edu/simx/index.html

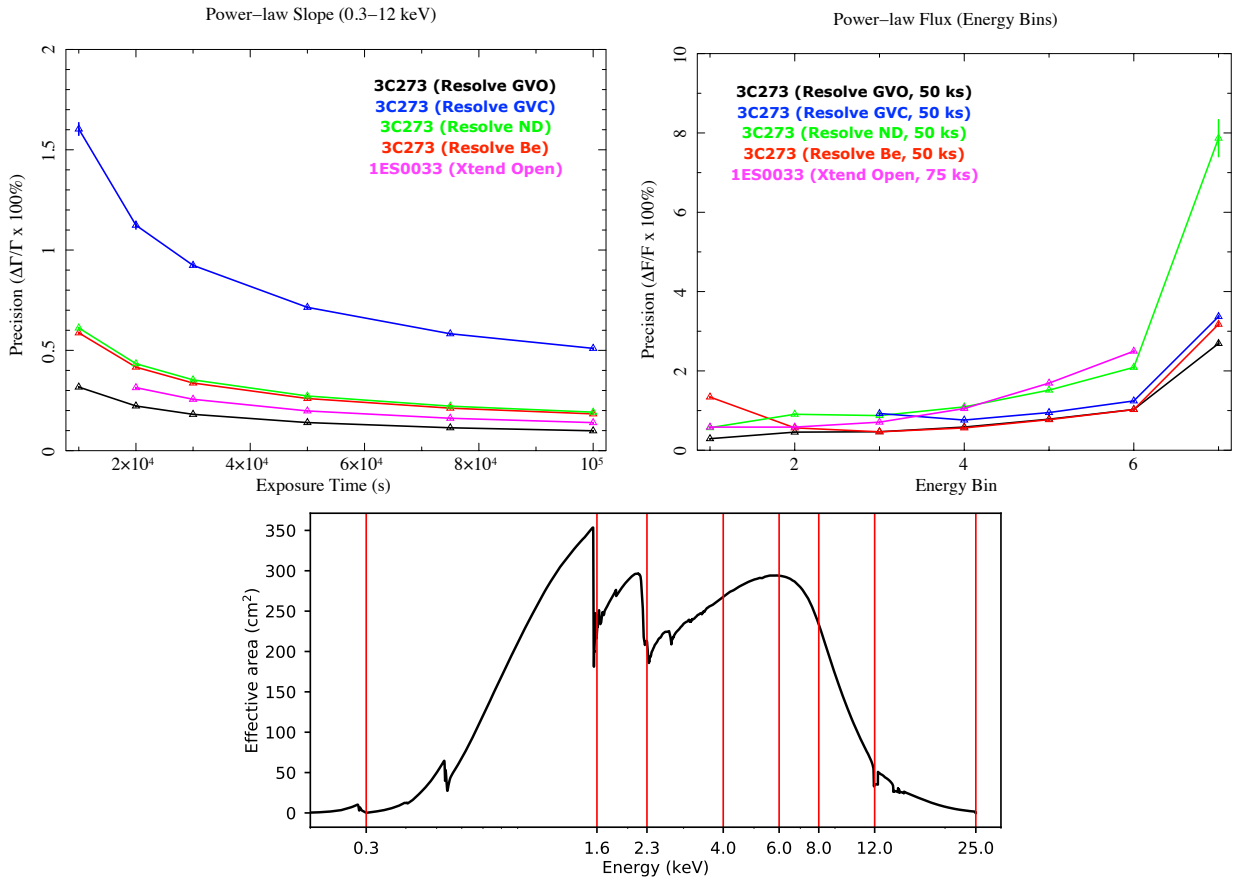

Figure 3. Simulation results for the proposed effective area primary calibration targets. Top left: Precision in constraining the power-law slope over the 0.3–12 keV energy band, as a function of exposure time. Top right: Precision in constraining the flux in individual energy sub-bands. Bottom: Expected effective area curve of Resolve, identifying the energy sub-bands used in the top right plot.

the instrumental background, assuming that the levels for Resolve and Xtend are similar to those measured in-flight for the Hitomi SXS and SXI, respectively, and the cosmic X-ray background (CXB) components.[39]

Based on these simulations, we examine the precision with which critical parameters of the source are constrained. In the case of a source dominated by a power-law component, we seek to recover the input spectral slope as well as the flux of the power-law. For the latter, we have examined the structure of the predicted effective area curve to define meaningful energy sub-bands in which the estimated flux can be best used to constrain and understand any deviations from the ground calibration baseline. These bands are 0.3–1.6 keV, 1.6–2.3 keV, 2.3–4.0 keV, 4.0–6.0 keV, 6.0–8.0 keV, 8.0–12.0 keV, and >12.0 keV (see Figure 3). For each observational set-up, we perform 10 different realisations of the corresponding simulation and average the fit results. Recovering the flux is complicated by the fact that the fit variable in this case is the normalization of the power-law at the energy of 1 keV, which is not within the energy range of all but one of the chosen sub-bands. To account for this issue, we apply the `cflux` model in XSPEC, which convolves with the power-law component to yield its flux in ergs cm^{-2} s^{-1} over an input energy range. The accuracy and precision of the flux are evaluated through a joint fit, with spectral slope free to vary but linked between the different energy sub-bands considered.

In order to ensure a 5% precision across most energy sub-bands, our simulations suggest that the optimal exposure times for each of the considered calibration sources and filter configurations are around 50–75 ks. Reaching a 5% precision and accuracy becomes challenging for high energies (> 8 keV), where a more careful modelling of the CXB will also play a role in recovering the correct input fluxes (and therefore higher investments of observing time bring diminishing returns). The results for our primary choice of calibrators, 3C273 for Resolve

and 1ES 0033+595 for Xtend, are illustrated in Figure 3. PKS 2155 and PSR 1509−58 are also suitable targets that should enable us to reach the Resolve calibration requirements if 3C273 is not visible at the appropriate time after the launch. 1ES 0033+595 will yield useful checks for the on-axis effective area of Resolve as well, and can be used to cross-calibrate the two different instruments onboard XRISM. Alternatively to 1ES 0033+595, G21.5−0.9 can be used for calibrating Xtend; however, the precision in the lowest energy bin is reduced given the high photoelectric absorption covering this source, and care must be taken because this SNR, while having a compact core, is extended at low surface brightness beyond the FOV of Resolve, making cross-calibration between the two instruments more difficult.

For the purpose of the calculations presented above, we have assumed the location of the optical axis is known, such that the calibration sources can be placed at the on-axis position during the observation. In fact, the determination of the optical axis, the off-axis effective area (vignetting curve), and the shape of the off-axis PSF are intimately interconnected, especially for Resolve, where the FOV is only a few times larger than the half-power diameter of the mirror PSF. The strategy for verifying these parameters in flight for Resolve is described in Section 4.4.1.

For Xtend, we plan to verify in flight the off-axis effective area and position of the optical axis that benefit from detailed measurements and modelling performed during ground calibration. To achieve this, observations of a cool core cluster of galaxies positioned at several off-axis and roll angles on the detector are the preferred method. This has the advantage that the intra-cluster medium is not time-variable, avoiding the need for expensive coordinated observations with other X-ray satellites to meet this calibration requirement. As potential targets, we consider bright galaxy clusters with a strongly peaked surface brightness profile, such as Abell 478, Abell 1795, Abell 2029, or PKS 0745−191. Of these, Abell 478 has the most compact core, and is therefore our primary target.

We estimated the surface brightness profile of Abell 478 by fitting an elliptical beta model to the corresponding XMM-Newton image of this cluster (ObsID 0109880101), and approximated its spectrum using a single-temperature, collisionally ionized plasma model modified by photoelectric absorption from the Milky Way. These spatial and spectral parameters are used as input for `heasim` Xtend simulations. Based on these simulations, exposure times of 10 ks per field are sufficient to detect the cluster core (within the central 1.8′ radius) with a signal-to-noise of more than 30 (precision $\sim 3.3\%$) up to the energy band of 8–12 keV and as far as 12′ off axis. We initially plan four observations of Abell 478, or any other compact cool core cluster with an appropriate visibility window: one observation placing the cluster core at the aimpoint, and three offset observations probing position angles of 0°, 90°, and 225° at off-axis angles of 8′, 8′, and 12′, respectively (see schematic in Figure 4). This is the minimum configuration that probes both positive and negative off-axis angles, and can identify 2D distortions of the vignetting curve. Fitting a 2D Lorentzian function to these measurements allows the optical axis position to be determined with an accuracy of $\pm 0.1'$ (see Figure 4). Should these measurements disagree significantly with the vignetting function and position of the optical axis determined from the ground calibration, for instance due to deformations of the mirror during launch, we will devise a more comprehensive plan to probe multiple position and off-axis angles in order to perform a full re-calibration.

The build-up of molecular contamination on cold surfaces within the light path is a serious concern for either instrument on XRISM, especially given the experiences of Suzaku[40] and Chandra.[41] Instrumental design features including the multi-stage thermal filters on Resolve and the warm, offset contamination blocking filter on Xtend are expected to prevent this, but we must still monitor for time-dependent effective area losses using the isolated neutron star RXJ 1856 and the compact SMC SNR 1E 0102.2−7219. This will include an observation very soon after the Resolve gate valve and Xtend door are opened to obtain a zero-contamination baseline. These flux-stable sources are complimentary and both are useful; RXJ1856 is a soft continuum source against which the absorption edges from carbon- and oxygen-rich contaminant can be easily measured by Resolve, while 1E 0102.2−7219 has a few isolated, bright emission lines above the oxygen edge whose flux can be quickly checked against a highly vetted and well-understood IACHEC model.[42] 1E 0102.2−7219 is always visible (see Figure 1), making it an ideal target to monitor the soft effective area. If contamination is found, an observing plan to characterize and calibrate it will be executed. This plan is still under development, but it will involve more frequent monitoring of similar sources, including the Cygnus Loop to measure off-axis build-up on Xtend, and a strategy such as that presented in Section 4.6.2 to understand the composition.

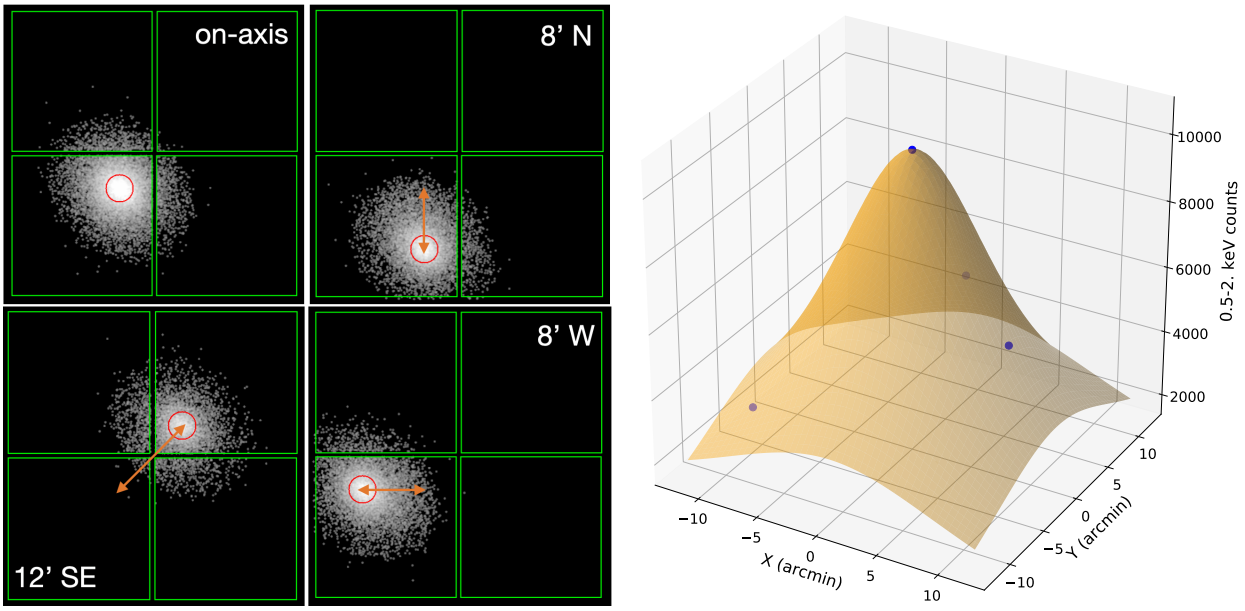

Figure 4. Left: Simulated 0.5–2.0 keV images of Abell 478 for the minimal four-pointing configuration proposed for verifying the off-axis effective area of Xtend in flight. The green squares mark the edges of the four Xtend CCDs. The images have been smoothed with a $\sigma = 5''$ Gaussian. All four images are shown using the same gray scale so that the slight dimming of the off-axis images with respect to the on-axis one visually represent the vignetting effect. Each pointing is 10 ks in length. Orange arrows show the displacement of the cluster peak from the optical axis. Right: source counts obtained from the central $1.8'$ radius of the cluster (red circles in the left panel) for each of the four observations, and the corresponding best-fit 2D Lorentzian function. The location of the peak of this function is used to identify the optical axis position.

4.4 PSF

XRISM will have a point spread function similar to that of Hitomi (Figure 5). Every point source will contribute significant scattered flux into regions of the detector (both Resolve and Xtend) far from its nominal location. Knowledge of the PSF shape, including its wings at distances far beyond the half-power radius, is particularly important for spectroscopy of extended sources with steeply declining radial brightness profiles, such as galaxy clusters and dust scattering halos around Galactic binaries, where the faint diffuse signal from the source outskirts can be overwhelmed by the scattered X-rays from the much brighter peak.

The XRISM PSF will be extensively calibrated on the ground, placing the source at multiple off-axis distances and azimuthal angles. For both mirrors, the PSF will be fully imaged with high spatial resolution. In orbit, we will need to (a) verify that there has been no change in PSF shape and (b) determine the position where the mirror optical axis crosses the detectors, which is the reference point for the PSF and effective area radial dependence. For Resolve, the small FOV places a serious constraint on both measurements.

4.4.1 Optical axis position

The optical axis position is defined as a position of the maximum throughput of the mirror. For Xtend, it can be determined by placing a constant compact source at several large offsets, where the throughput declines significantly, and fitting the position of the peak observed count rate (Section 4.3). For Resolve, we have only $\sim 1'$ offsets to work with, where the count rate declines by only 1.5–2% from the on-axis maximum. To detect such small relative variations, we need as bright a point source as possible (without saturating the detector). Bright point sources are inherently variable, so an independent simultaneous monitoring of its flux variability to $\ll 1\%$ precision will be needed. We will use LMC X-1, placing it at the center of the FOV and at five $1'$ offsets in a star-like pattern. A total of 30 ks (six 5-ks pointings) should allow us to determine the position of the peak throughput to a $15''$ accuracy.

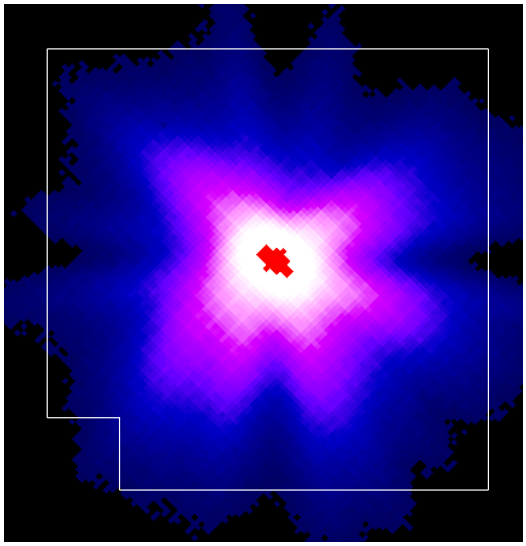

Figure 5. Image of the Hitomi on-axis PSF from ground calibration overlaid on the $3' \times 3'$ Resolve FOV (white outline). The XRISM PSF is expected to be similar. The PSF has a half-power diameter of $\sim 1.2'$, thus a point source will contribute significantly to all pixels of Resolve.

4.4.2 PSF shape and wings

The on-axis PSF, in which for our purposes we include on-axis as well as small offset pointings inside the Resolve FOV, will be verified using point sources observed for other purposes, such as Capella. The off-axis PSF (which is essentially the ratio of the wing brightness to that in the peak) is trickier, because when the peak is out of the Resolve FOV, we need an independent measure of the total source flux. Xtend will not be of help, because sources bright enough to measure the PSF wings will cause pile-up for Xtend. We will have to arrange for external simultaneous flux monitoring for the calibration sources.

For Resolve off-axis sources, the measured count rate is the product of the source sky flux times the off-axis effective area times the fraction of flux in the PSF wings that falls into the Resolve FOV. Unlike on the ground, the latter two quantities (off-axis area times PSF wings) cannot be disentangled in orbit. But fortunately, it is their product that is necessary for the spectral analysis of extended sources, and that is what we will verify in flight.

We plan to use two point sources, PKS 2155 for offsets $1.5'$–$3'$, and the brighter Cyg X-2 for offsets $5'$–$9'$, covering several interesting off-axis radii and azimuthal angles. Alternate sources for visibility are 3C273 and Mrk 421 (the jet in 3C273 will not have a significant effect). Modest exposures are required to reach the necessary statistical accuracy within the Resolve FOV. The data, i.e., the ratio of the counts from Resolve to the total flux from the external simultaneous measurement (properly normalized using on-axis pointings), will be compared with the prediction of the ray-tracing code, which will have been calibrated using the ground data. If significant systematic discrepancies are uncovered (meaning that the mirror has changed between the ground and the orbit), we will observe our calibration sources in a more comprehensive raster of off-axis positions and adjust the ray-tracing code to match the in-flight data.

For Xtend, we cannot use sources as bright as those for Resolve. We are planning to use fewer, longer observations of a fainter point source, possibly 1ES 0033+595.

4.5 Timing

XRISM has the same time assignment system as Hitomi.[43] For each Resolve event, an onboard time tag called the trigger time is assigned in the instrument-specific local time counter with resolution of 80 μs. In the ground data processing, a correction is applied, which converts the time counter from the trigger time to the most probable photon arrival time with resolution of 5 or 80 μs depending on the event grade.[27] It is then converted

to the spacecraft time coordinate using a lookup table in house-keeping data. For Xtend, the procedure is similar but the time tag is telemetered for each exposure sequence start. This means that the timing calibration of Xtend is essentially optimization of the exposure sequence start time.[26]

The timing calibration has two requirements: the absolute and relative timing (Table 1). For each, the timing error has contributions from both the satellite bus side and the instrument side, thus the requirements are defined for the mission as a whole. For Resolve, the trigger-time dependence on the event parameters such as the grade, pixel, and energy is the most important factor for the relative timing calibration (up to 1 ms before the correction), while the jitter of the spacecraft timing signal is normally small ($\lesssim 10$ μs) thanks to the GPS synchronization. For the absolute timing, both the spacecraft bus side and the instrument side can contribute in the form of propagation delay of the spacecraft timing signal and a systematic offset in the instrument's local time counter between the trigger time (after the correction of the event parameter dependence) and the most probable photon arrival time, respectively.

In the ground tests, the timing performance of the spacecraft bus and the instruments will be verified and calibrated separately to satisfy the timing error allocation for each, using actual GPS signals and pulsed X-rays of the MXS, respectively. This should establish the baseline timing calibration before launch. The goal of the in-flight timing calibration is primarily to cross-calibrate the absolute timing to other satellites or telescopes using coordinated observations of variable celestial sources e.g., pulsars, and secondly to verify the relative timing within an instrument (e.g., the trigger-time dependence correction for Resolve events) and between instruments. The calibration observations will be performed both in the initial calibration phase and in the normal observation phase as regular monitoring.

The baseline of the calibration target selection is largely inherited from the plan and result of the Hitomi calibration. The milli-second pulsar PSR B0540−69 and the accreting pulsar Cen X-3 were originally planned as the calibration targets for the SXS and SXI, respectively, but these were never observed. Instead, the Crab pulsar, the then primary calibration target for the hard X-ray instruments on Hitomi, was used for the timing calibration of both instruments. The high flux of the Crab enabled calibration of the SXS grade-dependent timing.[44] Combined with the 0.1-s burst-mode observation, it also allowed cross-calibration of the SXI timing with the technique using out-of-time events.[26]

For the XRISM timing calibration, the Crab pulsar will be the primary calibration target because this target alone enables us to achieve both the primary and secondary goals mentioned above. To determine backup targets for Resolve, eight pulsars were selected: the SXS target PSR B0540−69, three NuSTAR targets, PSR B1821−24, PSR J1937+21, and PSR J0218+4232,[45] and four NICER targets, PSR J0437−4715, PSR J0030+0451, PSR J1231−1411, and PSR J2124−3358.[46]

The timing accuracy is limited not only by the performance and calibration but also by a verification limit originating from observation-specific uncertainties such as statistical errors. The candidate targets were screened by exposure times that are required to make the statistical error on the pulse peak phase to be $\Delta t \lesssim 100$ μs at 3σ. This conservative threshold is chosen to allow sufficient margin for other anticipated uncertainty terms. For the current purpose, a simple order estimation using a Gaussian approximation of the peak profile should be sufficient for most cases. The statistical error is $\Delta t \propto \sigma_{\rm peak}/\sqrt{r_{\rm peak}\, t_{\rm exp}}$ and required exposure time is $t_{\rm exp} \propto \sigma^2_{\rm peak}/r_{\rm peak}$, where $\sigma_{\rm peak}$ and $r_{\rm peak}$ are the peak width and peak count rate, respectively. Thus, a sharp pulse profile as well as high pulse count rate is the key parameter.

The exposure times were derived by scaling the SXS result with the above relation, which are shown in Figure 6. The NICER targets (gray dots) do not have sufficiently bright or sharp pulses, and thus these were dropped from the candidate list. The NuSTAR targets (orange dots in bottom left) have sharp profiles, making these good backups despite their moderate brightnesses. On the other hand, the SXS target PSR B0540−69 (orange dot in top right), does not look promising owing to the broad profile and long pulse period of ~ 50 ms.[47] However, this is likely because this pulsar has rather a sinusoidal pulse profile, which makes the Gaussian approximation less valid. A more sophisticated approach, such as cross-correlation analysis, would improve the feasibility for this target. Therefore, it was decided to keep it as an alternative backup.

From the visibility perspective (Figure 1), PSR B0540−69 is the best; it is visible throughout the year. The three NuSTAR targets, if combined, also cover most of the year with an overlap with the Crab pulsar. Note

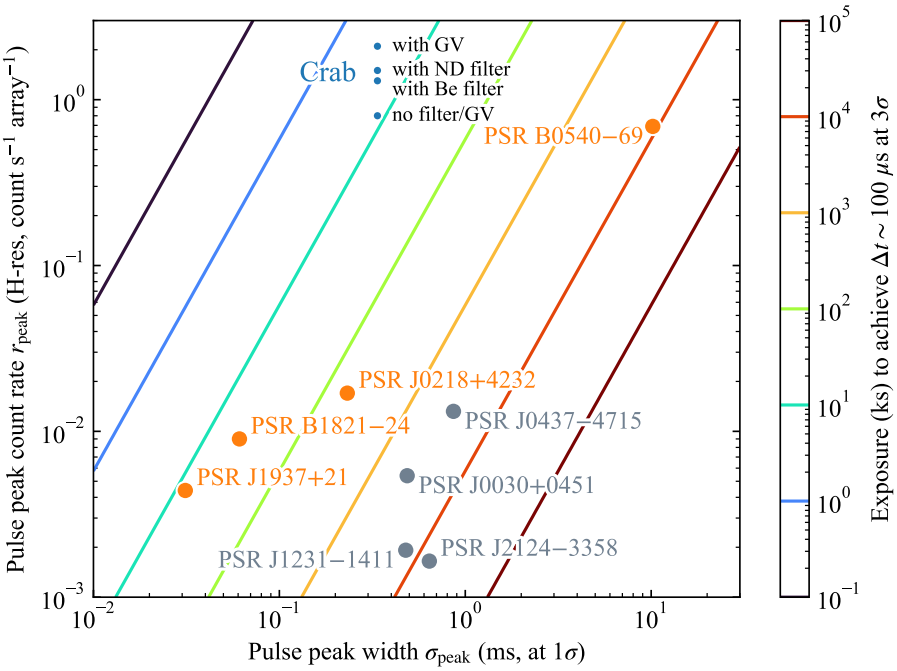

Figure 6. Required exposure times for the Resolve absolute timing calibration. Contours show the exposure time ($t_{\rm exp}$) required to achieve statistical uncertainty on the pulse peak phase of $\Delta t \sim 100$ μs at 3σ, which is a function of the peak count rate ($r_{\rm peak}$) and peak width ($\sigma_{\rm peak}$) of a pulsar. Dots show order estimation for candidate pulsars with a Gaussian approximation of pulse profiles. Only high-resolution (H-res) events are considered.

that, in the above evaluation, only the primary goal, the absolute timing calibration using high-resolution (H-res) grade events, is considered. The backup targets ($\lesssim$ 1 mCrab) are not bright enough to calibrate the Resolve relative timing, especially the grade dependence (having sufficient non-high-res branching ratio requires a source to be $\gtrsim$ 100 mCrab), or to cross-calibrate the Xtend timing using the out-of-time events technique. Therefore, additional calibration using, e.g., the MXS for Resolve and an accreting pulsar for Xtend may also be needed. As a next step of the planning, more accurate exposure-time estimation based on simulations is ongoing and discussion on coordinated observations is to be initiated soon.

4.6 Science Calibration

Like missions before it, XRISM will open up an unexplored arena in X-ray astrophysics, and we saw from Hitomi that this will challenge the fidelity of the very tools we need to understand the data.[8] We have adopted the concept of "science calibration" observations as a category of targets that, while they do not address a formal instrumental calibration requirement, and may not be as interesting astrophysically as other PV-phase targets, have the potential to greatly improve the science return of the mission. Examples of such observations being considered are presented below.

4.6.1 Atomic modeling

Large uncertainties on atomic constants (e.g., transition energies, cross sections) will lead to unacceptable errors on scientific results obtained from the observed spectra. There is an increasing demand that the spectral models and their atomic data should be sufficiently tested during the early mission phase, using observations of selected objects that contain relevant information for the atomic physics quantities. There have been discussions in the XRISM IFCP team and the laboratory astrophysics working group on possible targets and their value for laboratory astrophysics.

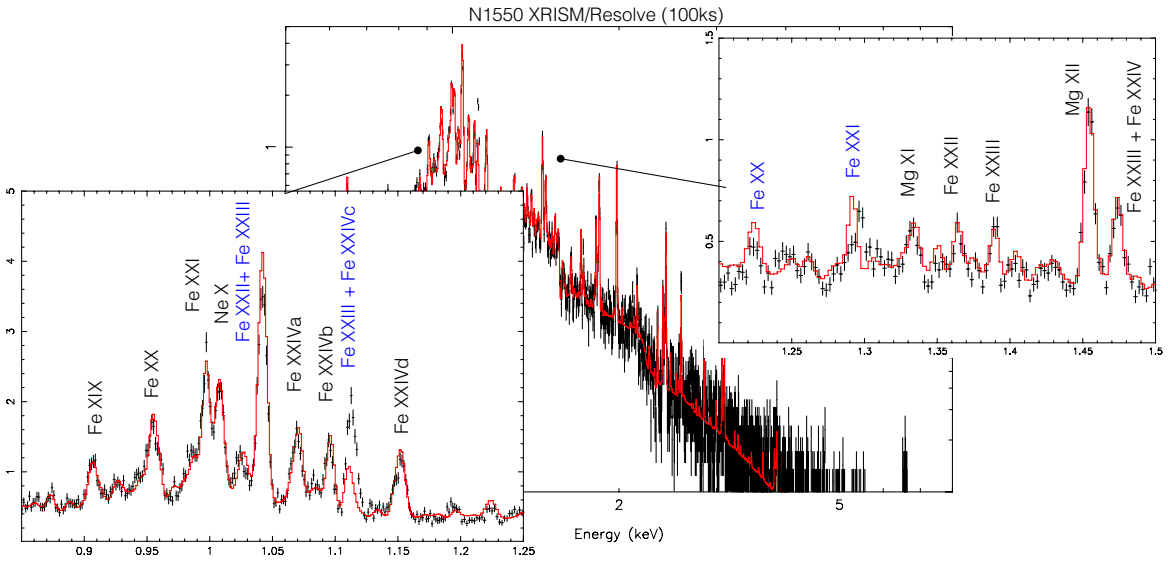

Figure 7. Simulated Resolve spectrum of NGC 1550. The simulation data (black) is based on APEC and the fit model (red) is from SPEX. The discrepancies on line emissivities and wavelengths that will be addressed at $> 3\sigma$ significance are shown in blue.

The preferred candidates are galaxy clusters or groups. They can be used for calibrating the collisional plasma model in ionization equilibrium. The other sources such as coronal stars have complex emission measure distributions, whereas hot gas in a region of a cluster or group can be almost isothermal. The Hitomi spectrum of the Perseus cluster has been a showcase for calibrating the atomic physics of 4-keV plasma, and now we will need similar measurements but for cooler plasma.

A main focus will be the Fe L-shell complex. Accurately modeling the Fe-L spectrum is known to be challenging due to the large number of transitions and physical processes involved in the detailed line formation. A number of XRISM proposals will depend on these lines, and thus early calibration and communication will be important for the community. One of the ideal candidates is NGC 1550, which is a relaxed group with a nearly isothermal temperature of 1.3 keV. It is optimal for benchmarking the line centers and cross sections of Fe XX–Fe XXIV at the L-shell, where the two main atomic codes (APEC and SPEX) have not yet fully converged (see Figure 7).

Alternative sources to NGC 1550 are the relaxed quasi-isothermal regions in M87 and Abell 1060, although their temperatures ($\sim$ 2–3 keV) are a bit too high for the Fe XX–Fe XXII. They are still useful for testing the energies and cross sections of Fe XXIII and Fe XXIV L-shell lines, as well as some of the K-shell lines at higher energies.

4.6.2 ISM X-ray absorption fine structure

If contaminant builds up between the time of ground-based effective area measurements and telescope first light, then the true effective area near photoelectric absorption edge fine structure will be significantly altered. This scenario was found to be the case for the XMM-Newton RGS,[48] where it is hypothesized that water ice built up as the instrument cooled from -50°C to -110°C. Such a phenomenon presents itself as additional, unidentified absorption features that are not easily attributed to the interstellar medium (ISM). De Vries et al. (2003)[49] demonstrated a technique for determining the new detector effective area in high resolution: compare the spectra of a low-ISM-column source ($N_{\rm H} \lesssim 10^{20}$ cm^{-2}) and a high-ISM-column source ($N_{\rm H} \gtrsim 10^{21}$ cm^{-2}) to verify that the residual absorption is not astrophysical in nature. By taking the ratio of the spectra, one can derive an empirical absorption spectrum for the ISM, normalized by $N_{\rm H}$. This measurement can serve as an empirical benchmark for studies of the cold ISM, calibrating the position of absorption edge structure relative to theoretical models, and correcting for interstellar extinction in high resolution.

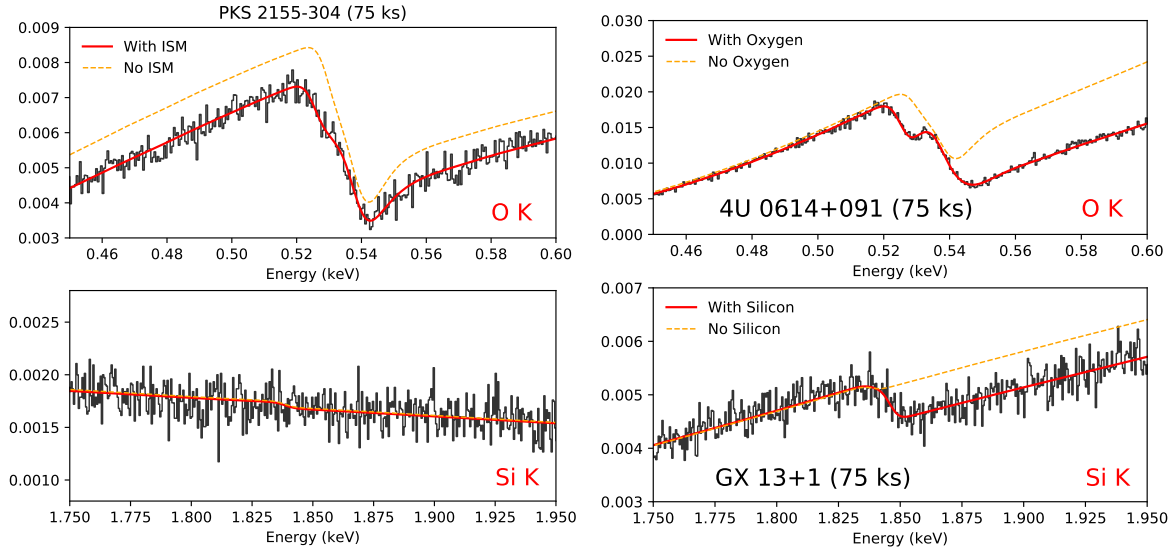

Figure 8. Simulated count rate histograms for potential calibration of the effective area fine structure. (Left) The blazar PKS 2155 has a low ISM column of $N_{\rm H} = 2\times10^{20}$ cm^{-2} and is expected to have some visible interstellar oxygen absorption in its spectrum. The optical depth from interstellar silicon is negligible. (Right) Simulated XRISM spectra of targets suitable for calibrating the instrumental response around the O K (4U 0614+091) and the Si K (GX 13+1) photoelectric edges. The dashed orange curves show the expected count rate absent of the relevant ISM absorption features, illustrating the expected instrumental response in each photoabsorption region.

Comparing two sources with different ISM columns is ideal for two reasons.[49] First, the empirical absorption spectrum for the ISM can be used to correct the low-ISM source in order to obtain $< 5\%$ precision on the final effective area results. Second, comparing two sources is necessary to identify features that are intrinsic to the physical properties of the sight line; for example, a 22.77 Å feature seen in quasar spectra but not in a spectrum of Sco X-1, which probes the local ISM.[49]

The XRISM IFCP team is focused on two photoelectric edge regions for spot-checking the accuracy of the ground-based effective area calibration: O K and Si K. We will first look for anomalies in the high resolution spectra of a low-ISM source such as 3C273, PKS 2155, or Mrk 421, which have $N_{\rm H} < 2\times10^{20}$ cm^{-2}. Only interstellar oxygen is expected to be detectable in these sources; the optical depth for neutral silicon will be $< 1\%$ (Figure 8, left). If found, we will proceed to observing a high-ISM-column source with a smooth spectrum in the range of interest. In the case of O K, a 50-ks observation of LMXB 4U 0614+091 ($N_{\rm H} \sim 3\times10^{21}$ cm^{-2}) will be sufficient. In the case of Si K, we will calibrate with a higher ISM column source like GX 3+1 or GX 13+1 ($N_{\rm H} \sim 1.6$–3×10^{22} cm^{-2}), which can be observed with the Resolve neutral density filter to avoid saturating the PSP (Figure 8, right).

5. SUMMARY

XRISM will continue a new era of spatially resolved, high-resolution X-ray spectroscopy begun by Hitomi. The unprecedented combination of spectral resolution and effective area over a broad X-ray band poses challenges for in-flight calibration that we have addressed in the preliminary calibration plan presented here. We emphasize the need for flexibility in this plan, including a set of secondary targets to reduce gaps in visibility when a particular calibration observation needs to be performed, and including the need to have a properly vetted plan in place well before it is needed in flight. This plan draws from the technical and scientific experience of the entire XRISM team, including Instrument and Science Team members, it builds on lessons learned from Hitomi, and it leverages the decades of experience with high-energy calibration that exist within the IACHEC. We expect the final plan to be crucial in realizing the mission's ambitious science goals.

ACKNOWLEDGMENTS

XRISM is being developed under an international collaboration of the Japan Aerospace Exploration Agency (JAXA), the National Aeronautics and Space Administration (NASA), and the European Space Agency (ESA). We acknowledge the efforts of the instrument teams of XRISM, Hitomi, Suzaku, and ASTRO-E, whose work over the past two decades and more has lead to such an exciting mission. We especially thank members of the Hitomi In-Flight Calibration Planning Team who have moved on from XRISM, and whose efforts have greatly informed the XRISM plan. We finally thank members of the IACHEC, whose dedication in ensuring the best calibration maximizes the science we learn from these missions. Part of this work was performed under the auspices of the U.S. Department of Energy by Lawrence Livermore National Laboratory under Contract DE-AC52-07NA27344.

REFERENCES

[1] Tashiro, M., Maejima, H., Toda, K., et al., "Concept of the X-ray Astronomy Recovery Mission," in [*Society of Photo-Optical Instrumentation Engineers (SPIE) Conference Series*], **10699**, 1069922 (July 2018).

[2] Tashiro, M. S., Maejima, H., Toda, K., et al., "Status of X-Ray Imaging and Spectroscopy Mission (XRISM)," in [*Society of Photo-Optical Instrumentation Engineers (SPIE) Conference Series*], **11444**, 11444176 (Dec. 2020).

[3] Takahashi, T., Kokubun, M., Mitsuda, K., et al., "Hitomi (ASTRO-H) X-ray Astronomy Satellite," *Journal of Astronomical Telescopes, Instruments, and Systems* **4**, 021402 (Apr. 2018).

[4] Hitomi Collaboration et al., "The quiescent intracluster medium in the core of the Perseus cluster," *Nature* **535**, 117–121 (July 2016).

[5] Aharonian, F. A., Akamatsu, H., Akimoto, F., et al., "Hitomi Constraints on the 3.5 keV Line in the Perseus Galaxy Cluster," *Astrophysical Journal* **837**, L15 (Mar. 2017).

[6] Hitomi Collaboration et al., "Solar abundance ratios of the iron-peak elements in the Perseus cluster," *Nature* **551**, 478–480 (Nov. 2017).

[7] Hitomi Collaboration et al., "Hitomi observations of the LMC SNR N 132 D: Highly redshifted X-ray emission from iron ejecta," *Publications of the Astronomical Society of Japan* **70**, 16 (Mar. 2018).

[8] Hitomi Collaboration et al., "Atomic data and spectral modeling constraints from high-resolution X-ray observations of the Perseus cluster with Hitomi," *Publications of the Astronomical Society of Japan* **70**, 12 (Mar. 2018).

[9] Hitomi Collaboration et al., "Detection of polarized gamma-ray emission from the Crab nebula with the Hitomi Soft Gamma-ray Detector," *Publications of the Astronomical Society of Japan* **70**, 113 (Dec. 2018).

[10] Hitomi Collaboration et al., "Hitomi X-ray studies of giant radio pulses from the Crab pulsar," *Publications of the Astronomical Society of Japan* **70**, 15 (Mar. 2018).

[11] Hitomi Collaboration et al., "Search for thermal X-ray features from the Crab nebula with the Hitomi soft X-ray spectrometer," *Publications of the Astronomical Society of Japan* **70**, 14 (Mar. 2018).

[12] Hitomi Collaboration et al., "Hitomi X-ray observation of the pulsar wind nebula G21.5-0.9," *Publications of the Astronomical Society of Japan* **70**, 38 (June 2018).

[13] Hitomi Collaboration et al., "Glimpse of the highly obscured HMXB IGR J16318-4848 with Hitomi," *Publications of the Astronomical Society of Japan* **70**, 17 (Mar. 2018).

[14] Hitomi Collaboration et al., "Hitomi observation of radio galaxy NGC 1275: The first X-ray microcalorimeter spectroscopy of Fe-Kα line emission from an active galactic nucleus," *Publications of the Astronomical Society of Japan* **70**, 13 (Mar. 2018).

[15] Hitomi Collaboration et al., "Measurements of resonant scattering in the Perseus Cluster core with Hitomi SXS," *Publications of the Astronomical Society of Japan* **70**, 10 (Mar. 2018).

[16] Hitomi Collaboration et al., "Temperature structure in the Perseus cluster core observed with Hitomi," *Publications of the Astronomical Society of Japan* **70**, 11 (Mar. 2018).

[17] Hitomi Collaboration et al., "Atmospheric gas dynamics in the Perseus cluster observed with Hitomi," *Publications of the Astronomical Society of Japan* **70**, 9 (Mar. 2018).

[18] Nandra, K., Barret, D., Barcons, X., et al., "The Hot and Energetic Universe: A White Paper presenting the science theme motivating the Athena+ mission," arXiv:1306.2307 (June 2013).

[19] Gaskin, J. A., Swartz, D. A., Vikhlinin, A., et al., "Lynx X-Ray Observatory: an overview," *Journal of Astronomical Telescopes, Instruments, and Systems* **5**, 021001 (Apr. 2019).
[20] Nakajima, H., Hayashida, K., Tomida, H., et al., "Soft x-ray imager (SXI) for Xtend onboard X-Ray Imaging and Spectroscopy Mission (XRISM)," in [*Society of Photo-Optical Instrumentation Engineers (SPIE) Conference Series*], **11444**, 11444177 (Dec. 2020).
[21] Porter, F. S., Eckart, M. E., Leutenegger, M. A., et al., "Initial ground calibration of the Resolve detector system on XRISM," in [*Society of Photo-Optical Instrumentation Engineers (SPIE) Conference Series*], **11444**, 11444178 (Dec. 2020).
[22] Midooka, T., Tsujimoto, M., Kitamoto, S., et al., "X-ray transmission measurements of the gate valve for the X-ray astronomy satellite XRISM," in [*Society of Photo-Optical Instrumentation Engineers (SPIE) Conference Series*], **11444**, 11444285 (Dec. 2020).
[23] Terada, Y., Holland, M., Loewenstein, M., et al., "Detail plans and preparations for the science operations of the XRISM mission," in [*Society of Photo-Optical Instrumentation Engineers (SPIE) Conference Series*], **11444**, 11444286 (Dec. 2020).
[24] Loewenstein, M., Hill, R. S., Holland, M. P., et al., "The XRISM science data center: Optimizing the scientific return from a unique x-ray observatory," in [*Society of Photo-Optical Instrumentation Engineers (SPIE) Conference Series*], **11444**, 11444287 (Dec. 2020).
[25] Eckart, M. E., Leutenegger, M. A., Okajima, T., Hayashi, T., Mori, H., Maeda, Y., Tsujimoto, M., and de Vries, C., "XARM Resolve Calibration Requirements (RESOLVE-SYS-REQ-0017)," (2018).
[26] Nakajima, H., Maeda, Y., Uchida, H., et al., "In-orbit performance of the soft X-ray imaging system aboard Hitomi (ASTRO-H)," *Publications of the Astronomical Society of Japan* **70**, 21 (Mar. 2018).
[27] Ishisaki, Y., Yamada, S., Seta, H., et al., "In-flight performance of pulse-processing system of the ASTRO-H/Hitomi soft x-ray spectrometer," *Journal of Astronomical Telescopes, Instruments, and Systems* **4**, 011217 (Jan. 2018).
[28] Sembay, S., Guainazzi, M., Plucinsky, P., and Nevalainen, J., "Defining High-Energy Calibration Standards: IACHEC (International Astronomical Consortium for High-Energy Calibration)," in [*X-ray Astronomy 2009; Present Status, Multi-Wavelength Approach and Future Perspectives*], Comastri, A., Angelini, L., and Cappi, M., eds., *American Institute of Physics Conference Series* **1248**, 593–594 (July 2010).
[29] Kilbourne, C. A., Adams, J. S., Brekosky, R. P., Chervenak, J. A., Chiao, M. P., Eckart, M. E., Figueroa-Feliciano, E., Galeazzi, M., Grein, C., Jhabvala, C. A., Kelly, D., Leutenegger, M. A., McCammon, D., Scott Porter, F., Szymkowiak, A. E., Watanabe, T., and Zhao, J., "Design, implementation, and performance of the Astro-H SXS calorimeter array and anticoincidence detector," *Journal of Astronomical Telescopes, Instruments, and Systems* **4**, 011214 (Jan. 2018).
[30] de Vries, C. P., Haas, D., Yamasaki, N. Y., et al., "Calibration sources and filters of the soft x-ray spectrometer instrument on the Hitomi spacecraft," *Journal of Astronomical Telescopes, Instruments, and Systems* **4**, 011204 (Jan. 2018).
[31] Guainazzi, M., David, L., Grant, C. E., Miller, E., Natalucci, L., Nevalainen, J., Petre, R., and Audard, M., "On the in-flight calibration plans of modern x-ray observatories," *Journal of Astronomical Telescopes, Instruments, and Systems* **1**, 047001 (Oct. 2015).
[32] Sambruna, R. M., Brandt, W. N., Chartas, G., Netzer, H., Kaspi, S., Garmire, G. P., Nousek, J. A., and Weaver, K. A., "X-Ray Imaging of the Seyfert 2 Galaxy Circinus with Chandra," *Astrophysical Journal* **546**, L9–L12 (Jan. 2001).
[33] Bianchi, S., Matt, G., and Iwasawa, K., "The circumnuclear X-ray reflectors in NGC 1068 and the Circinus galaxy," *Monthly Notices of the Royal Astronomical Society* **322**, 669–680 (Apr. 2001).
[34] Yaqoob, T., Serlemitsos, P., Mushotzky, R., et al., "The X-Ray Emission of 3C 273 Observed with ASCA," *Publications of the Astronomical Society of Japan* **46**, L49–L53 (June 1994).
[35] Ishida, M., Tsujimoto, M., Kohmura, T., Stuhlinger, M., Smith, M., Marshall, H. L., Guainazzi, M., Kawai, K., and Ogawa, T., "Cross Spectral Calibration of Suzaku, XMM-Newton, and Chandra with PKS 2155-304 as an Activity of IACHEC," *Publications of the Astronomical Society of Japan* **63**, S657–S668 (Nov. 2011).
[36] Marsden, D., Blanco, P. R., Gruber, D. E., Heindl, W. A., Pelling, M. R., Peterson, L. E., Rothschild, R. E., Rots, A. H., Jahoda, K., and Macomb, D. J., "The X-Ray Spectrum of the Plerionic System PSR B1509−58/MSH 15−52," *Astrophysical Journal* **491**, L39–L42 (Dec. 1997).

[37] de la Calle Pérez, I., Bond, I. H., Boyle, P. J., et al., "Search for High-Energy Gamma Rays from an X-Ray-selected Blazar Sample," *Astrophysical Journal* **599**, 909–917 (Dec. 2003).

[38] Nynka, M., Hailey, C. J., Reynolds, S. P., et al., "NuSTAR Study of Hard X-Ray Morphology and Spectroscopy of PWN G21.5-0.9," *Astrophysical Journal* **789**, 72 (July 2014).

[39] Bautz, M. W., Miller, E. D., Sanders, J. S., et al., "Suzaku Observations of Abell 1795: Cluster Emission to r_{200}," *Publications of the Astronomical Society of Japan* **61**, 1117 (Oct. 2009).

[40] Koyama, K., Tsunemi, H., Dotani, T., et al., "X-Ray Imaging Spectrometer (XIS) on Board Suzaku," *Publications of the Astronomical Society of Japan* **59**, 23–33 (Jan. 2007).

[41] Plucinsky, P. P., Bogdan, A., Marshall, H. L., and Tice, N. W., "The complicated evolution of the ACIS contamination layer over the mission life of the Chandra X-ray Observatory," in [*Society of Photo-Optical Instrumentation Engineers (SPIE) Conference Series*], *Society of Photo-Optical Instrumentation Engineers (SPIE) Conference Series* **10699**, 106996B (July 2018).

[42] Plucinsky, P. P., Beardmore, A. P., Foster, A., Haberl, F., Miller, E. D., Pollock, A. M. T., and Sembay, S., "SNR 1E 0102.2-7219 as an X-ray calibration standard in the 0.5-1.0 keV bandpass and its application to the CCD instruments aboard Chandra, Suzaku, Swift and XMM-Newton," *Astronomy & Astrophysics* **597**, A35 (Jan. 2017).

[43] Terada, Y., Yamaguchi, S., Sugimoto, S., et al., "Time assignment system and its performance aboard the Hitomi satellite," *Journal of Astronomical Telescopes, Instruments, and Systems* **4**, 011206 (Jan. 2018).

[44] Leutenegger, M., Audard, M., Boyce, K., et al., "In-flight verification of the calibration and performance of the ASTRO-H (Hitomi) Soft X-ray Spectrometer," *Journal of Astronomical Telescopes, Instruments, and Systems* **4**, 021407 (Apr. 2018).

[45] Gotthelf, E. V. and Bogdanov, S., "NuSTAR Hard X-Ray Observations of the Energetic Millisecond Pulsars PSR B1821-24, PSR B1937+21, and PSR J0218+4232," *Astrophysical Journal* **845**, 159 (Aug. 2017).

[46] Bogdanov, S., Guillot, S., Ray, P. S., et al., "Constraining the neutron star mass–radius relation and dense matter equation of state with NICER. i. the millisecond pulsar x-ray data set," *The Astrophysical Journal* **887**, L25 (Dec. 2019).

[47] Campana, R., Mineo, T., De Rosa, A., Massaro, E., Dean, A. J., and Bassani, L., "X-ray observations of the Large Magellanic Cloud pulsar PSR B0540-69 and its pulsar wind nebula," *Monthly Notices of the Royal Astronomical Society* **389**, 691–700 (Sept. 2008).

[48] de Vries, C. P., den Herder, J. W., Gabriel, C., Gonzalez-Riestra, R., Ibarra, A., Kaastra, J. S., Pollock, A. M. T., Raassen, A. J. J., and Paerels, F. B. S., "Calibration and in-orbit performance of the reflection grating spectrometer onboard XMM-Newton," *Astronomy & Astrophysics* **573**, A128 (Jan. 2015).

[49] de Vries, C. P., den Herder, J. W., Kaastra, J. S., Paerels, F. B., den Boggende, A. J., and Rasmussen, A. P., "The interstellar oxygen-K absorption edge as observed by XMM-Newton. Separation of instrumental and interstellar components," *Astronomy & Astrophysics* **404**, 959–967 (June 2003).